RESEARCH ARTICLE | JUNE 15 2020

Rotational state-changing collisions of C$_2$H$^-$ and C$_2$N$^-$ anions with He under interstellar and cold ion trap conditions: A computational comparison ⊘

Jan Franz ; Barry P. Mant ; Lola González-Sánchez ; Roland Wester ; Franco A. Gianturco ✉

Check for updates

View Online   Export Citation   CrossMark

Rotational state-changing collisions of C₂H⁻ and C₂N⁻ anions with He under interstellar and cold ion trap conditions: A computational comparison

View Online   Export Citation   CrossMark

Jan Franz,[1] [ID] Barry P. Mant,[2] [ID] Lola González-Sánchez,[3] [ID] Roland Wester,[2] [ID] and Franco A. Gianturco[2,a] [ID]

AFFILIATIONS

[1] Department of Theoretical Physics and Quantum Informatics, Faculty of Applied Physics and Mathematics,
Gdańsk University of Technology, ul. Narutowicza 11/12, 80-233 Gdańsk, Poland

[2] Institute for Ion Physics and Applied Physics, University of Innsbruck, Technikerstr. 25/3, 6020 Innsbruck, Austria

[3] Departamento de Química Física, University of Salamanca, Plaza de los Caídos s/n, 37008 Salamanca, Spain

[a] Author to whom correspondence should be addressed: francesco.gianturco@uibk.ac.at

ABSTRACT

We present an extensive range of quantum calculations for the state-changing rotational dynamics involving two simple molecular anions that are expected to play some role in the evolutionary analysis of chemical networks in the interstellar environments, C_2H^- ($X^1\Sigma^+$) and C_2N^- ($X^3\Sigma^-$), but for which inelastic rates are only known for C_2H^-. The same systems are also of direct interest in modeling selective photo-detachment experiments in cold ion traps where the He atoms function as the chief buffer gas at the low trap temperatures. This study employs accurate, *ab initio* calculations of the interaction potential energy surfaces for these anions, treated as rigid rotors, and the He atom to obtain a wide range of state-changing quantum cross sections and rates at temperatures up to about 100 K. The results are analyzed and compared for the two systems to show differences and similarities between their rates of state-changing dynamics.

Published under license by AIP Publishing. https://doi.org/10.1063/5.0011585

I. INTRODUCTION

The discovery of carbon chain anions in interstellar and circumstellar media has triggered and stimulated a large number of theoretical and experimental studies on these species (e.g., see Refs. 1–3). Their structures and spectral features, as well as the clarification of their importance and of their role in interstellar chemistry and in gas phase ion–molecule reactions in general, have therefore also attracted many specific studies[4–6] on their behavior. Recent examples have been our experimental work on the absolute photodetachment (PD) cross section measurements for hydrocarbon chain anions,[7] which has been nicely matched and confirmed by a computational study of the same systems.[8]

The possible, and likely, existence of anions in astrophysical sources was first predicted theoretically and considered in earlier chemical models,[9,10] although the first negative hydrocarbon C_6H^- was only detected in 2006,[11] thereby also solving the problem of the unidentified lines discovered by Kewaguchi *et al.*[12] This identification was soon followed by the detection of other negatively charged species, such as C_4H^-,[13] C_8H^-,[14,15] C_3N^-,[16] C_5N^-,[17] and CN^-.[18] The majority of these species were first detected in a well-observed Circumstellar Envelope (CSE) IRC+10216, although these and other hydrocarbon anions were also discovered later on in other molecular clouds.[19] As to be expected, the study and search for interstellar anions of both simple and increasingly more complex structural properties are still current and relevant. More specifically, a simple species, such as C_2H^- ($X^1\Sigma^-$), has been expected to be amenable

to observation with the new astrophysical instruments such as atacama large millimeter/submillimeter array (ALMA), especially since it had already been observed as a stable molecule in laboratory experiments.[20,21] Furthermore, its parent neutral form C_2H ($X^2\Sigma^+$) has already been a well-known astrophysical molecule discovered by observation as early as 1974,[22] thereby suggesting that the corresponding C_2H^- anion should also be present, although perhaps as only a very low-abundance species, a fact justified in terms of its high chemical reactivity and therefore expected rapid destruction upon formation. In fact, actual current numerical models predict that the formation of larger carbon chain anions should in any case be more probable than that for similar but smaller chains as the C_2H^-,[23] hence somehow supporting the difficulties for its observation.

The detection of carbon chain anions and parent neutral species in various astronomical environments has stimulated many computational studies of their collisions with He and H_2 to obtain rotationally inelastic excitation and de-excitation rates. Examples include the series C_2H/C_2H^-,[24–27] C_4H^-,[28] C_6H/C_6H^-,[29,30] CN/CN^-,[31–36] and C_3N/C_3N^-.[37–39]

Despite that the actual origin of many of the hydrocarbon anions has not yet been solved, it is generally accepted that gas-phase processes are crucial for their formation and therefore the many observed hydrocarbon radicals C_nH may also be the main precursors for the formation of C_nH^- anions through electron attachment or association processes, whereas associative detachment processes would contribute to the generation of initial, neutral C_nH species. As an example, a new mechanism for the formation of C_2H^- from C_2H_2 had been proposed not long ago[1] from laboratory experiments. Recent experiments in our group have also investigated the reactions of C_2H^- with C_2H_2 as a means of forming larger $C_{2n}H^-$ and C_{2n} chains.[40]

Along similar lines, another small C-bearing molecule, the neutral C_2N radical ($X^2\Pi_r$), had also been detected earlier on in the interstellar medium,[41] where the molecule was observed at the 1–2 mK level toward the same circumstellar envelope (CSE) of IRC+10216 already mentioned earlier, using the facilities of the Arizona Radio Observatory (ARO). Lambda doublets of the $J = 4.5 \rightarrow 3.5$ and the $J = 6.5 \rightarrow 5.5$ transitions at 106 GHz and 154 GHz in the $\Omega = 1/2$ ladder were measured with the ARO 12 m telescope, as well as the $J = 9.5 \rightarrow 8.5$ lines near 225 GHz, using the ARO Sub-Millimeter Telescope (SMT).[41] Considering other species in the same environment, it is interesting to note that the [CN]/[C$_2$N]/[C$_3$N] abundance ratio was found to be ~500/1/50, thus indicating again that one could expect a rather low abundance for the neutral radical C_2N. For the corresponding anionic counterpart, however, no observational evidence within the same CSE has been reported thus far, also suggesting a low abundance of the latter once formed within this chemical network.

Despite this absence of direct detection, both the above anionic molecules, C_2N^- and C_2H^-, have been the object of several laboratory studies, which have analyzed in some detail the photo-detachment (PD) mechanisms of these species and several other structural properties.[42–47] Furthermore, in general terms, we should note here that possible astrophysical abundances of either observed or not yet observed species have to be understood in terms of molecular stabilities, reaction probabilities, and of both radiative and collisional excitations and relaxation of internal molecular modes: the accurate knowledge of all these facts can indeed help us to better explain the existence of a molecule and the probability of it being observed. The molecular stability and the spectroscopic properties of both the C_2H^- and C_2N^- anions have been studied in various earlier investigations,[42,43,47] while the modeling of molecular emission in the interstellar medium (ISM) environments where they could be expected to exist requires collisional rate coefficients with the most abundant interstellar species such as He and H_2. Collisional data have already been presented for the C_2H^- anion interacting with He,[27] while no corresponding calculations, as far as we know, exist for the collisional rotation-state changes of C_2N^- interacting with He. The actual *ab initio* potential energy surface (PES) is also not known for this system. The quantum dynamics of both these anions, besides not being extensively studied under CSE conditions, has also been only partially discussed under the operating low temperatures of ion cold traps.[48] The present work is therefore directed to acquiring novel knowledge about the quantum dynamics of C_2N^- in collision with He under both astrochemical and cold ion trap conditions, further implementing a comparison between its dynamical behavior and that of the C_2H^- polar anion under similar conditions.

Section II only briefly reminds readers about the features of the anisotropic potential energy surface involving C_2H^- and He atoms, since it has been presented and analyzed already in earlier work.[27] It instead presents in greater detail the new calculations of the *ab initio* points related to the Rigid Rotor (RR) PES associated with the interaction between C_2N^- ($X^3\Sigma^-$) and the neutral He atom. The two interaction potentials will then be compared, and their level of spatial anisotropy will be analyzed and discussed.

Section III presents the state-changing rotationally inelastic cross sections for both systems and discusses the effects from spin–spin and spin–rotation structural features on the C_2N^- system vis-à-vis the C_2H^- ($X^1\Sigma^+$) system. The corresponding inelastic rates at the temperatures of interest are also presented, compared, and discussed. Section IV examines the possible evolutionary dynamics of C_2N^- anions under the conditions of a cold trap when they are undergoing laser-driven photo-detachment processes. A comparison with the corresponding behavior of the C_2H^- system is also presented and discussed. Conclusions are given in Sec. V.

II. FEATURES OF THE *AB INITIO* INTERACTIONS OF C_2H^- AND C_2N^- WITH He ATOMS

The electronic ground state of C_2N^- was taken to be ($X^3\Sigma^-$) as indicated in earlier work.[43] The molecular geometry of this linear anion is $r_{CC} = 1.344$ Å and $r_{CN} = 1.207$ Å and was given in the experiments from Garand *et al.*[43] We have optimized the molecular geometry using the multi-reference configuration interaction (MRCI) + Davidson correction[49,50] employing the aug-cc-pVQZ[51] basis set obtaining $r_{CC} = 1.360$ Å and $r_{CN} = 1.212$ Å. The *ab initio* calculations of the 2D grid of points in Jacobi coordinates (R, θ) were carried out with the program package MOLPRO 2012.[49,50] For all the present calculations, we have employed the internally contracted multi-reference configuration interaction method (IC-MRCI),[52,53] using the aug-cc-pVQZ basis set[51] on all atoms. The

reference space for the MRCI calculations consists of a complete active space by distributing 14 electrons in 15 orbitals. All single and double excitations from the reference configurations are included in the variational calculation. The effect of quadruple excitations is estimated via the Davidson correction.[49,50] Since the MRCI approach does not provide a size-consistent method, we have included a correction for size-consistency by using the Davidson correction that estimates the contributions of quadrupole excitations, as discussed in Refs. 54 and 55. The Basis-Set-Superposition-Error (BSSE) correction was not included in this study because this procedure is not well defined when multi-reference methods are employed. In any event, our previous experience with small anions interacting with He has shown us that the corresponding rigid-rotor PES is only marginally modified by BSSE corrections in the well regions and on the onset of the repulsive walls. We therefore expect that it would also be not very significant in the present case. We further checked the quality of the asymptotic form of the interaction by calculating the corresponding potential term for the situation where He approaches with an angle of 90° to the molecular axis. In this situation, the terms of the potential involving the higher order Legendre polynomial should be zero (by symmetry) and the spherical part should dominate. The computed value of the coefficient for the asymptotic potential gives us the value of the spherical polarizability of the He atom, which comes out to be $1.379\ a_0^3$. This value is in good agreement with a recent result from QED calculations[56] of 1.383 760 78.

To further test possible differences coming from our different post-Hartree–Fock methods we have used, we have carried out a comparison between MRCI(Q) and perturbative estimate of the energy contribution from triples (CCSD-T) calculations for the approach of the He partner at an angle of 90° with respect to the axis of the C_2N^- ion. In the comparison, the potential energy curves for CCSD-T and MRCI(Q) are set to zero at 25 Å. We found that both curves have their minimum at 3.5 Å, with the largest difference between the two curves occurring at the location of the minimum configuration: $-59.9\ cm^{-1}$ for CCSD-T compared to $-54.5\ cm^{-1}$ for MRCI(Q).

The angular grid involved calculations of radial "cuts" every 5° from 0° to 180°. The radial grid included a higher density of points around the various minima regions at each selected angle. A total of 44 radial points were used between 2.3 Å and 26 Å. We have not included the basis-set-superposition-error procedure because such a procedure turns out not to be well defined for multi-reference methods. The global minimum for the complex was found at a distance of around 3.545 Å from the center-of-mass, located at an angle of around 80°, with a well depth of around 58 cm^{-1}. The data shown by the two panels of Fig. 1 provide a pictorial view of the new PES calculated for the C_2N^-/He system (upper panel), while it also shows, for comparison, the PES already calculated in earlier work for the similar anion of C_2H^- interacting with He.[27] One sees in the two panels the similarities between the two interaction potentials since both exhibit the presence of a minimum energy region of their complex with He. The more shallow well of the lower panel is extensively off the C_{2v} geometry, while the deeper well on the upper panel appears to be more localized and closer to the center-of-mass than it is the case in the lower panel. Given the larger number of electrons in the C_2N^- case, the corresponding well is therefore deeper than that of the C_2H^-/He complex[27] and more
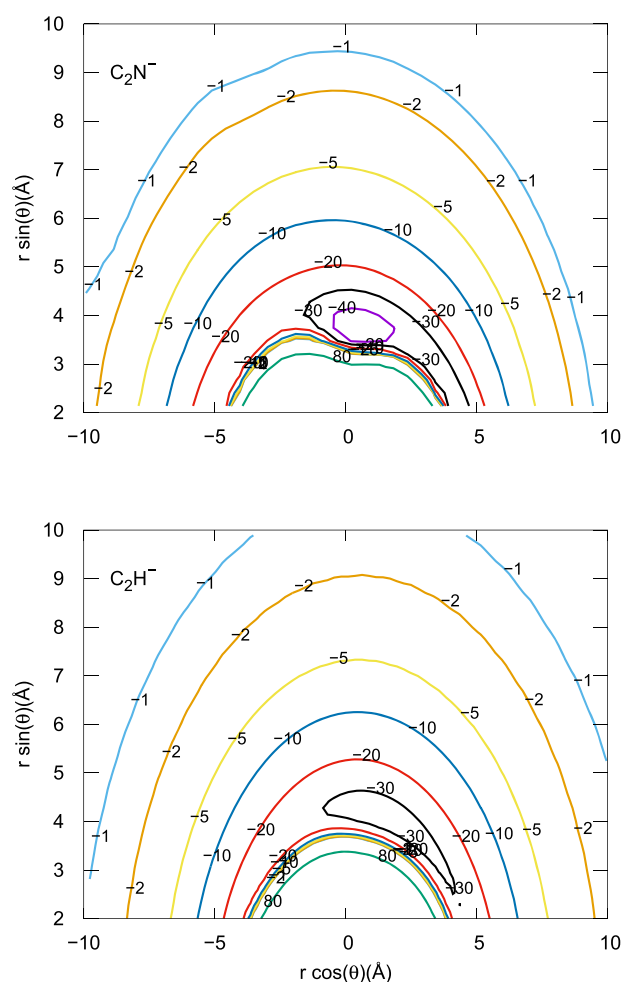

FIG. 1. Computed PESs for the two molecular anions of the present study. The data are presented as in-plane maps in 2D with $r\cos\theta$ and $r\sin\theta$ as coordinates. Energy levels in cm^{-1}. Upper panel: C_2N^- from present calculations and lower panel: C_2H^- from Ref. 27.

localized in space. Both potentials will be asymptotically driven by the polarizability term involving the spherical, dipole polarizability of the He partner and therefore will behave very similarly in their long-range regions because of it. The differences in their short-range features, however, will be reflected later in the size differences between their collisional state-changing probabilities discussed in Sec. III.

The localization of the excess charge provided by the extra bound electron of the anion is also an interesting item for the new C_2N^-/He PES presented here. The Mulliken charges in the asymptotic situation (e.g., with the helium at a distance of 26.55 Å from the center-of-mass of the anionic target) turn out to be as follows (when computed with the MRCI/aug-cc-pVQZ of the post-HF treatment): $C_1 = -0.590\ 49$, $C_2 = +0.225\ 32$, and $N_1 = -0.634\ 83$. Here, C_2 is the central carbon atom so that the geometry of C_2N^- is given as

C_1–C_2–N_1 with no extra charge on the interacting He atom, as expected. The direction and value of the dipole moment are therefore given as 2.1818 D, placed along the positive direction of the molecular z-axis from the C_1-end of the molecule, a result from the delicate balance between excess charges in this molecule. One should also note that the approach of the He atom along the direction of $0°$ is on the N-side of the C_2N^- anion. The same angle corresponds to the approach on the H-side of the C_2H^-. Another type of presentation of the PESs for both systems, to be used in the scattering calculations below, is obtained by numerically generating the radial coefficients of the multipolar expansion of the Rigid Rotor (RR) 2D potential energy surfaces,

$$V(r = r_e, R, \theta) = \sum_\lambda V_\lambda(R) P_\lambda(\cos\theta), \quad (1)$$

where r_e is the geometry of the equilibrium structure of the anion and the sum over the contributing λ values went up to 19, although only the dominant, stronger terms are shown in Fig. 2. The panels

of this figure also compare the present findings for C_2N^- with the earlier data for C_2H^-.[27] The expansion coefficients for the C_2N^-–He PES are provided in the supplementary material.

The radial coefficients presented in Fig. 2 underline once more both the general similarities between the two systems and important differences, which will vary their dynamical behavior we shall analyze below. If we look at the spatial anisotropy of the multipolar coefficients, we see that the spherical terms ($\lambda = 0$) are very similar to each other in both strength and spatial extension around their well regions. On the other hand, the radial coefficients with $\lambda = 1, 2$, and 4 are all uniformly repulsive in the short-range region for C_2H^-, while only those for $\lambda = 2$ and 4 are so for the C_2N^- anion. These differences indicate that the ΔN transitions between rotational levels, those for which the acting torques from the anisotropic PES coefficients will be stronger, could be those with ΔN with odd values for C_2N^- and with even values for the C_2H^-. The presence of such possible propensity effects will be further discussed when analyzing the computed inelastic cross sections and rates in Sec. III. Another important elements of distinction/similarity are the relative spacings in energy between the rotational states for both systems, which are presented in Fig. 3.

To simplify the comparison, we report only the energy spacing between N-level separations, without showing the spin–spin and
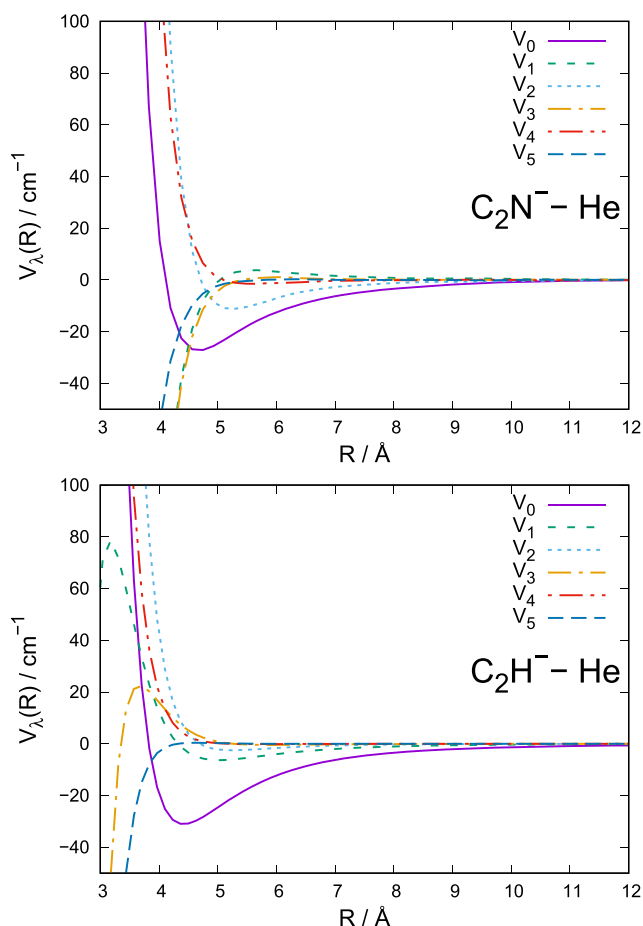

FIG. 2. Computed multipolar coefficients calculated from the initial PES data. Upper panel: lower values of the dominant radial coefficients for the C_2N^- anion and lower panel: same data but for the C_2H^- anion. Energy values are in cm^{-1} and distances in Å.
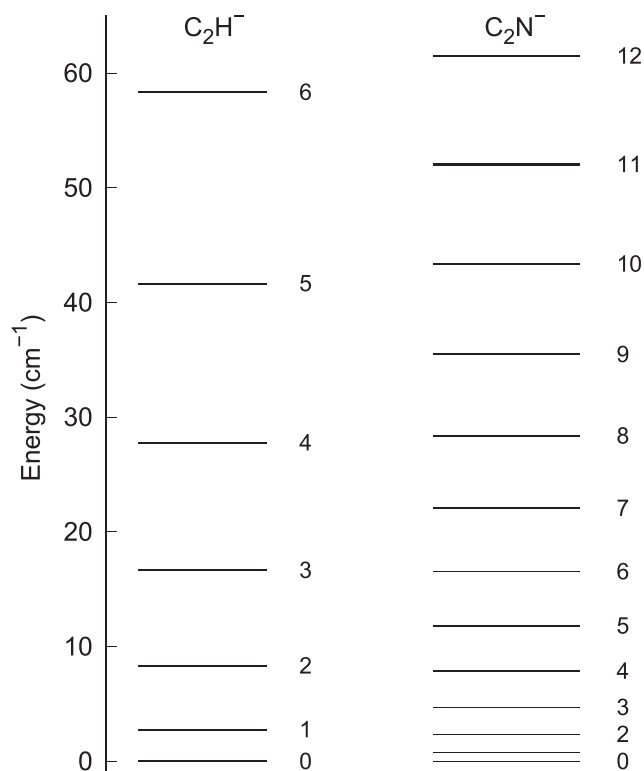

FIG. 3. Schematic location of the rotational energy levels for the molecular anion of the present study. For the case of C_2N^- ($X^3\Sigma^-$), only the pseudo-singlet levels without splitting effects are shown (see the main text for further details).

spin–rotation splitting for C_2N^-. The sizes of these splitting constants are not known or available as yet, and we will be discussing further in Sec. III how their effects will be included in the dynamics of the present study. Their energy splittings would in any event not be visible on the chosen energy scale in this figure. We clearly see, however, that the density of states over the examined range of about 60 cm^{-1}, which should cover most of the relevant energy range of the CSE environments and of the cold ion trap operation, is

FIG. 4. Steady-state distributions of relative molecular populations of rotational levels for temperatures up to 30 K. Upper panel: the C_2N^- anion and lower panel: the C_2H^- anion (see the main text for further discussion).

dramatically different between the two systems, with the C_2N^- anion showing twice as many states being accessible within this energy range. The markedly higher "crowding" of rotational states per unit energy for the latter molecule translates into a higher number of them being significantly populated at equilibrium temperatures in either environments.

The use of a Local Thermal Equilibrium (LTE) population scheme is often employed as a starting condition of ISM kinetic modelings. Additionally, photo-detachment experiments in cold traps usually start, as we shall further discuss in a Sec. IV, with thermal equilibrium of the molecular internal states being achieved at the temperature of the trap. A comparison between steady-state rotational level populations, over the range of temperatures of interest, is reported for the two anions by the two panels in Fig. 4. We clearly see in them that, as an example, at temperatures in a cold trap around 25 K, the C_2N^- anion in the left panel significantly populates levels up to $N = 10$, while the C_2H^- anion on the right panel only has states up to $N = 6$ significantly populated. Such differences of behavior will be further discussed in Secs. III and IV when the inelastic cross sections and rates will be computed first to numerical convergence and then the possible dynamics of laser-induced PD processes in traps will be analyzed at low temperatures.

Since the efficiency of state-changing collisional processes for rotational states is affected, among other features also discussed below, by the size of the energy gaps between the involved levels, we shall therefore expect that the marked differences shown in Fig. 3 will be reflected in differences between inelastic rates for the two anions.
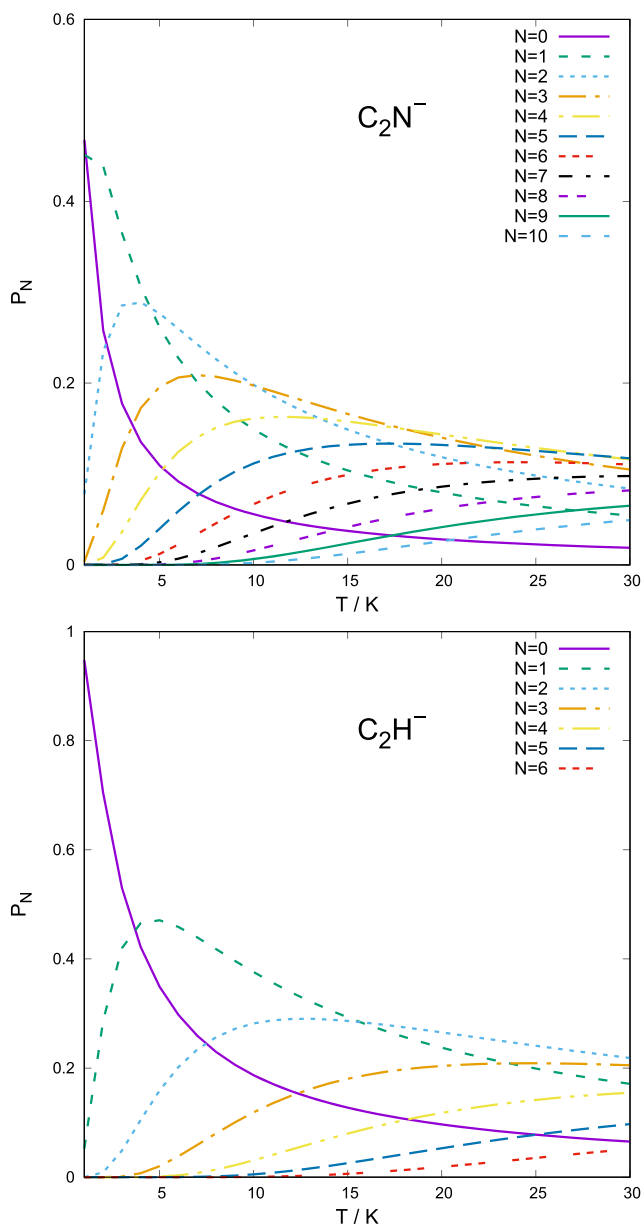
III. QUANTUM CALCULATIONS OF STATE-CHANGING ROTATIONALLY INELASTIC CROSS SECTIONS AND RATES

The inelastic cross sections involving collisional transitions in both the title molecules were calculated using our in-house multichannel quantum scattering code ASPIN, which we have already described in many earlier publications of our group[57–60] and therefore will not be repeated here in detail. Interested readers are referred to the above publications for consultation.

The ground state of the C_2N^- anion is $^3\Sigma^-$, the same as the OH^+ molecule for which we have previously studied low-temperature collisions with He in detail.[61,62] The conclusions of this previous work inform the calculations presented here. In the OH^+ ($^3\Sigma^-$) state, we have three levels for each total angular momentum ≥ 1: the rotational levels are in fact split by spin–spin and spin–rotation coupling effects. In the pure Hund's case (b), the electronic spin momentum S couples with the nuclear rotational angular momentum N to form the total angular momentum j, given by $j = N + S$.[61,62] As a consequence of this coupling term, the rotational levels of the molecule may be labeled not only by the above quantum numbers defined in the Hund's case (b) but also by their parity index ε. The levels in molecules of odd multiplicity with parity index equal to +1 are labeled **e**, and those with parity index equal to −1 are labeled **f**.[61] However, we shall omit this index in the following discussion since we shall not be using it in our analysis.

The extensive work we have done on collision of He with the OH$^+$ ($^3\Sigma^-$) molecule[61,62] has already shown that the $\Delta N \neq 0$ transitions involve much larger energy values than those which cause changes in the spin quantum number S that is responsible for the separations between j states. Thus, one can say that rotational quenching transitions have much larger energy gaps than those which simply cause spin-flipping processes within each N-labeled manifold. In a full close-coupling (CC) approach to the quantum dynamics, the molecular Hamiltonian includes, in addition to the rotational contribution, a nuclear coupling contribution, which induces hyperfine energy splitting. These splittings are however lower than typically 10^{-3} cm^{-1}, i.e., they are much lower than the rotational spacings investigated in this work, as we shall further show later in this paper. In such a situation, a possible approach would be to neglect the hyperfine splitting and to decouple the spin wave functions from the rotational wave functions using an angular momenta recoupling scheme (e.g., see Ref. 63), which simplifies considerably the dynamics of the problem. The latter is then reduced to solving the simpler spin-less CC equations associated with the more usual $^1\Sigma$ case. This approximate approach of treating the target as a pseudo-singlet case has been found in earlier works of our group[59,62] to yield results very close to the exact cross sections. Hence, the "recoupling approach" outlined above will be considered as our reference approach in the following calculations, where our results will be compared with those carried out for the exact $^1\Sigma$ case of the C$_2$N$^-$ molecular anion.

For C$_2$N$^-$–He (reduced mass $\mu = 3.619$ amu), scattering calculations were carried out for collision energies between 1 cm^{-1} and 500 cm^{-1} using steps of 0.05 cm^{-1} for 0–6 cm^{-1}, 0.1^{-1} for 6–100 cm^{-1}, 0.2 cm^{-1} for 100–200 cm^{-1}, 1.0 cm^{-1} for 200–400 cm^{-1}, and 2 cm^{-1} for 400–500 cm^{-1}. This fine energy grid was used to ensure that important features such as the many resonances appearing in the cross sections were accurately accounted for, and their contributions correctly included when the corresponding rates were calculated, as discussed below. The CC equations were propagated between 1.7 Å and 100.0 Å in 2000 steps using the log-derivative propagator[64] up to 60 Å and the variable-phase method at larger distances[58] up to 100 Å. The potential energy was interpolated between calculated $V_\lambda(r_{eq}|R)$ values using a cubic spline and extrapolated below and above the *ab initio* grid using linear and polynomial functions, respectively, as implemented in ASPIN.[57] As our *ab initio* grid goes to 26 Å and the scattering energies of interest are not in the ultracold or high energy regimes, the details of the potential extrapolation have a negligible effect on the scattering cross sections. To test this point, however, we have always extended the radial integration with an extrapolated potential of the R^{-4}-type out to 100 Å or more to reach convergence of the final cross sections. We have also found that to employ the correct dipole polarizability coefficient for the extrapolated potential instead of the value produced by ASPIN from the *ab initio* potential only changed the final cross sections by less than 1.0%, and only at the lowest energies. The rotational basis set was increased with increasing energy from $N = 20$ to $N = 36$ at the highest energy considered. The number of partial waves was also increased with increasing energy reaching $J = 96$ at the highest energy. Inelastic cross sections were computed for all transitions between $N = 0$ and $N = 15$, which was deemed to be sufficient to model buffer gas dynamics in a cold trap up to about 50 K (see below), while the same range of levels is expected to be

the one most significantly populated during low-energy collisional exchanges with He atoms within ISM environments dynamical conditions. Scattering calculations for C$_2$H$^-$ were carried out by us in a former study[48] using the PES of Dumouchel *et al.*[27] as discussed above.

Another quantity that we shall compute from the cross sections is the state-to-state inelastic rotational rates over a range of temperatures from thresholds up to about 100 K to cover the range of T values expected to be significant for processes in the ISM environments we are discussing here. Hence, once the state-to-state inelastic integral cross sections are known, the rotationally inelastic rate constants $k_{N \to N'}(T)$ can be evaluated as the convolution of the cross sections over a Boltzmann distribution of the relative collision energies. In the following equation, all quantities are given in atomic units:

$$k_{N \to N'}(T) = \left(\frac{8}{\pi \mu k_b^3 T^3} \right)^{1/2} \int_0^\infty E \sigma_{N \to N'}(E) e^{-E/k_B T} dE. \quad (2)$$

Both the calculations of inelastic cross sections and of their corresponding rates over the range of temperatures mentioned earlier have been carried out using the new interaction PES for the C$_2$N$^-$/He system and via the earlier PES already computed for the C$_2$H$^-$/He system.[27] The comparison between our findings for these two systems will be carried out below by presenting our computed data.

The present results for the inelastic cross sections, over a range of 100 cm^{-1}, are reported in the four panels of Fig. 5. The upper two panels show excitation processes, while the lower two panels present de-excitation cross sections for both systems. The solid lines refer to the calculations for C$_2$N$^-$, while the dashed lines are those for C$_2$H$^-$.

It is interesting to note that in the low-energy range up to about 20 cm^{-1} all of the cross sections reported in the four panels show the evidence of resonance effects in both systems. The relative strength of the interaction potentials and the presence of many more rotational states available for the C$_2$N$^-$ make the cross sections for the latter anion exhibit a much denser sequence of resonant features, as expected from the larger mass of the molecular partner (hence, a larger number of partial waves contributing to shape resonances) and form the stronger coupling with the nearby closed channels during the scattering (hence, the presence of Feshbach resonances). Since no experiments are as yet available on the scattering behavior of these anions, we shall not carry out any detailed analysis of the features seen in our calculations. They will however contribute to changing the size of the related inelastic rates we shall further discuss later and will be taken into account in our calculations.

In the upper two panels where excitation processes are reported, we see that in the left panel, showing $\Delta N = 1$ transitions, at energies beyond the resonance regions, the excitation from the lowest rotational state of C$_2$H$^-$ is the largest over the whole range, despite that the amount of energy transferred between levels is also the largest. Two structural factors could contribute to this dynamical difference: (i) the smaller value by about 30% of the reduced mass of the C$_2$H$^-$, which affects relative sizes of wavevectors, and (ii) the presence for only this molecule of an attractive well in the radial coefficient with $\lambda = 1$, which directly couples the levels involved in
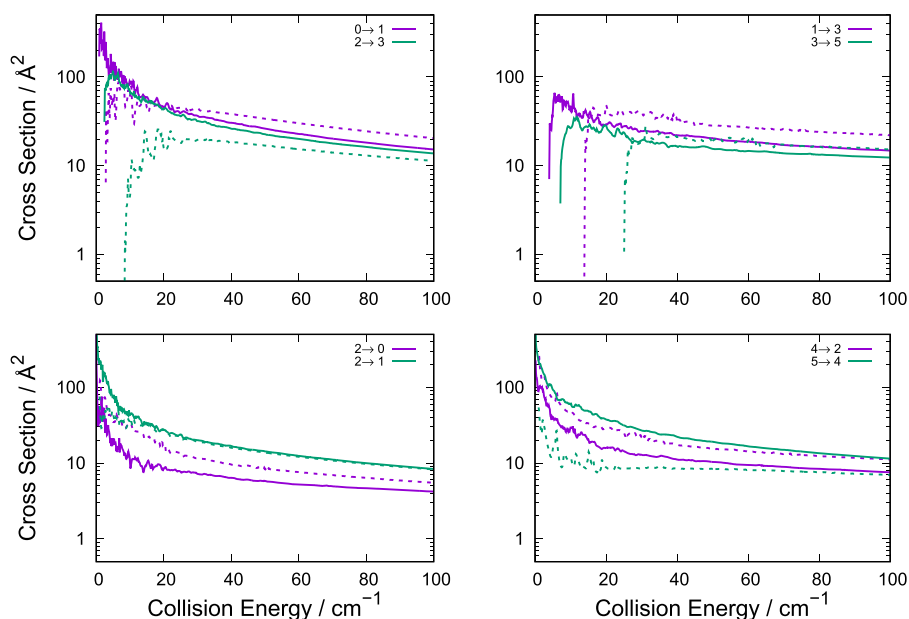
FIG. 5. Rotationally inelastic cross sections for the C_2N^- (solid lines) and the C_2H^- (dashed lines) anions. The upper panels report excitation processes, while the lower panels describe de-excitation processes (see the main text for further discussion).

that transition during collision. The marked increase in energy gap when one considers transitions still with $\Delta N = 1$ but between excited states (i.e., between the $j = 2$ and $j = 3$ levels) for the C_2H^- system in the same upper-left panel, is the dominant factor, which causes that inelastic cross section to be the smallest. On the other hand, the two excitation cross sections involving the same levels but for the C_2N^- anion, which are in that same panel, are closer to each other. This is due to the much smaller energy gap between its levels, which does not offset the greater strength of the interaction potential for the latter molecule compared to the former, hence making the C_2N^- anion more efficiently excited by collisions with He to its upper rotational states.

The upper-right panel of Fig. 5 shows now excitation processes involving $\Delta N = 2$ transitions. In the low-energy resonance regions, the cross sections are uniformly smaller than those discussed before for the C_2N^- anion, while those for the C_2H^- anion are instead larger in size and also larger than those pertaining to the other anion. This difference can be linked to the differences in behavior between their corresponding multipolar coefficients, as shown in Fig. 2. The C_2H^- partner presents both terms with $\lambda = 1$ and $\lambda = 2$ with marked attractive wells and steeply repulsive walls, while the other anion only shows this behavior for the $\lambda = 2$ coupling term. It therefore follows that both direct and indirect potential coupling effects are dynamically efficient for the C_2H^- anion, while only one is effective for C_2N^-.

When turning to the collisional de-excitation processes in the lower panels of Fig. 5, we see in the left panel that the transitions with $\Delta N = -1$ for the C_2N^- and the C_2H^- anions yield markedly larger cross sections than those for de-excitation transitions with $\Delta N = -2$, a behavior attributed again to the role played by the increase in the energy gaps in the case of the latter processes. In addition, the differences in the coupling strength between the two PESs discussed

earlier cause the $\Delta N = -2$ transitions for C_2N^- to be the smallest of them all. It is also interesting to note that, in the lower-left panel, the smallest of the cross sections is that for the $\Delta N = -1$ transition of the C_2H^- partner. The much larger energy gain transferred into relative energy between collision partners makes this system have a reduced interaction time, which, in turn, makes sudden collisions more effective. Since such a gain is larger for $\Delta N = -2$ processes than for the $\Delta N = -1$ transition, it makes sense that the cross sections for the latter are smaller than those for the former process when C_2H^- is concerned. The differences in energy gains are however much smaller for C_2N^-, where the differences between multipolar coefficients play a more important role than the smaller changes in the interaction times, thus making the $\Delta N = -1$ transitions to be the larger ones.

On the whole, the present quantum calculations of the relative state-changing collision probabilities for the two title systems indicate a clear similarity of general behavior and of relative efficiency for such processes at the energies of interest for ISM conditions, although changes linked to their structural features can distinguish between their interactions with the He atom and play a significant role in their relative dynamics.

The results reported by Fig. 6 indicate in the behavior of the rotationally inelastic collisional rates over a range of temperature covering values of interest for cold ion traps and also for ISM environments where the present anions are expected to be present. As with the cross sections of Fig. 5, the upper two panels report excitation processes, while the lower two panels show the behavior of the de-excitation processes. Solid lines refer to the C_2N^- anion, while the dashed lines are for the C_2H^- case.

It is interesting to note, when looking at the results in the two upper panels, that the differences in size between rates for $\Delta N = 1$ and those for $\Delta N = 2$ are fairly small in the case of the C_2N^- target
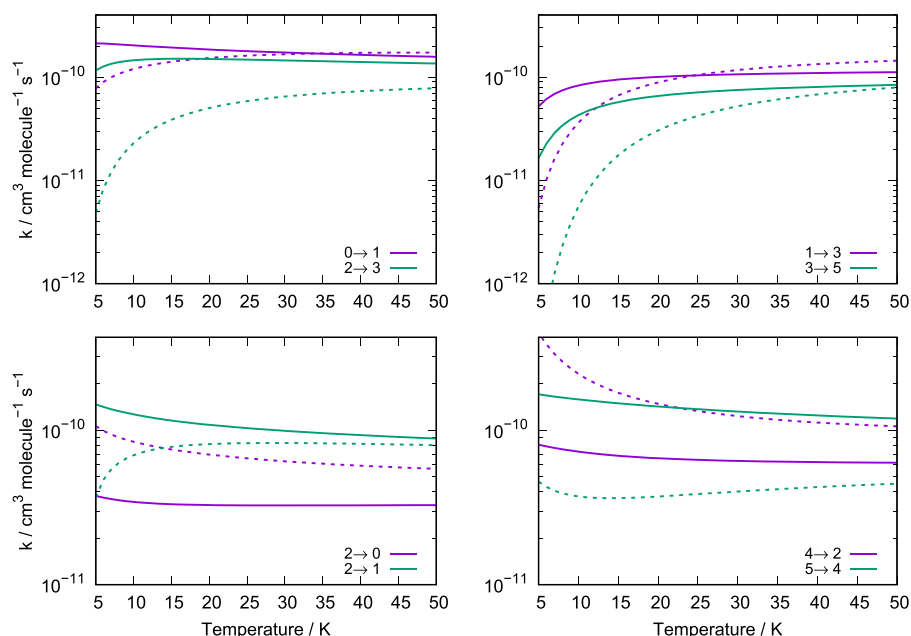
FIG. 6. Rotationally inelastic collisional rates for the C_2N^- (solid lines) and the C_2H^- (dashed lines) anions. The upper panels report excitation processes, while the lower panels describe de-excitation processes. The range of temperatures goes up to 50 K (see the main text for further discussion).

while are markedly larger for C_2H^- as a target. This is again due to the greater effects of the energy gaps between rotational states, which exist between the two anions, as shown in Fig. 3. These types of differences are also present in the de-excitation rates reported by the two lower panels, where again we see that the differences in size of the rates for each of the anion are all within less than one order of

magnitude. As expected, we see that the rates follow closely the indicated differences discussed earlier between cross sections for both systems.

The data reported by the four panels of Fig. 7 make a pictorial comparison between sizes of specific rate values at two different temperatures: at 15 K in the two upper panels and at 50 K in the two
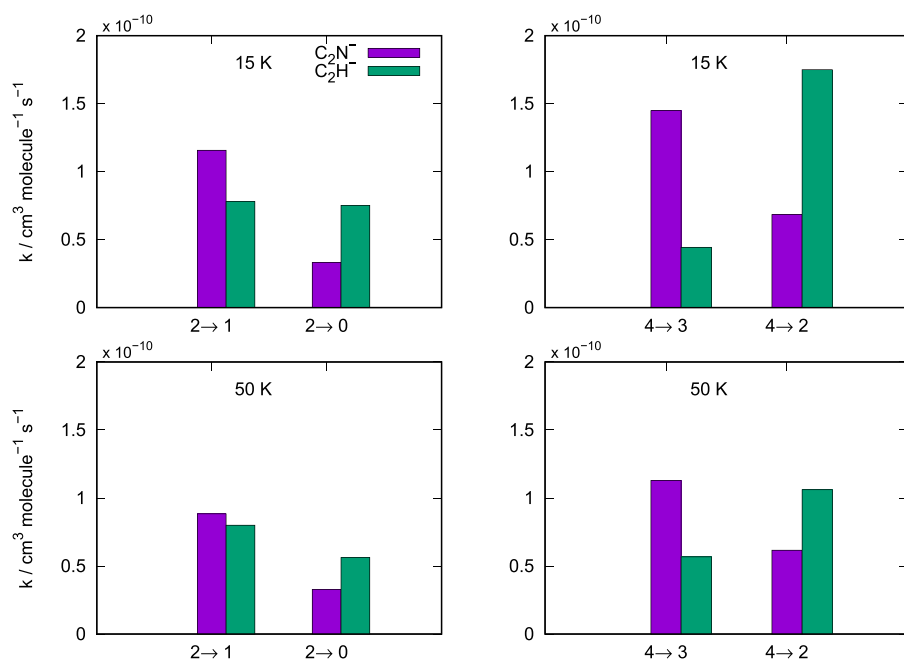

FIG. 7. Rotationally inelastic collisional quenching rates for the C_2N^- and C_2H^- anions for $N = 2$ (left panel) and $N = 4$ (right panel) at 15 K (top panels) and 50 K (bottom panels) (see the main text for further discussion).

lower panels. They confirm what was discussed earlier and underline the delicate interplay between the structural and dynamical differences controlling the state-changing collisions between rotational states in the two anions.

The upper two panels of Fig. 7 compare two de-excitation rates for two different initial states: $N = 2$ in the left panel and $N = 4$ in the right panel. The following comments can be made:

(i) the rates for the C_2N^- anion are larger for $\Delta N = -1$ processes while becoming smaller than those for C_2H^- for $\Delta N = -2$ processes. The switching is related to the differences in multipolar coefficients discussed earlier.

(ii) for the same types of transitions at the higher temperature shown in the lower two panels, we see that the inversion of relative magnitudes when going from $\Delta N = -1$ processes to the $\Delta N = -2$ is still present and linked to different coupling strengths of their state-changing dynamics.

Indicators on possible propensity rules for the size-dependence of the cooling (de-excitation) rates from an initial rotational state and down to different final levels are reported in the two panels of Fig. 8. The variations in size of the rates from the initial $N = 8$ to all final levels below are shown at two different temperatures.

Figure 8 verifies directly what we have already discussed when analyzing the cross sections and the rates, i.e., those in the collisional cooling (de-excitation) cascades within each system are linked to the differences in the structural features of the interactions between the anionic partners and the He atom. It is immediately clear that temperature does not play a significant role and that structural features are largely driving the differences. In the case of the C_2N^- anion, increasing the ΔN values down the ladder uniformly reduces the size of the inelastic rates as the energy gaps uniformly increase. Such differences are smaller than those for C_2H^- where larger energy spacings occur between levels. Within this decrease in size, however, we still see that for C_2N^-, the transitions involving odd ΔN values are larger than those with even values, while the opposite is true for the C_2H^-. This is again linked to the dynamical couplings

induced by the attractive $\lambda = 1, 3$, and 5 odd terms of the multipolar expansion of the C_2N^-, as shown in Fig. 2. On the other hand, for the C_2H^- anion, we see an even more marked effect linked to the relative strength of the multipolar coefficients (see again Fig. 2), since the $\lambda = 2$ and 4 potential coupling terms have a shallow attractive well in the outer radial range and become strongly repulsive around the turning point values at the energies of interest. We therefore see that they induce rotational torques during dynamics, which would favor transitions into final states where even ΔN values occur.

It follows from the above considerations that collisional repopulation of rotational levels will take different preferential paths in the two title systems, a result that would suggest the final presence in the relevant environments of different populations for their molecular rotational states.

Rates for all transitions between $N = 0$ and $N = 8$ for C_2H^- and between $N = 0$ and $N = 15$ for C_2N^- are provided in the supplementary material for temperatures between 0 K and 100 K.

IV. MODELLING QUANTUM DYNAMICS OF LASER PHOTO-DETACHMENT PROCESSES IN COLD TRAPS

One of the important processes, which can take place in cold ion traps[48,65] where molecular anions can be confined, involves studying the internal state evolution under laser-induced detachment of the extra anionic electron. The study of the photo-detachment of molecular anions is obviously more complicated than for atomic PD processes due to the increasing number of accessible pathways, which become available in the case of molecular targets. Molecules exhibit a higher density of lower-lying electronic states while one must further consider the increase in the density of states due to the additional vibrational motion, i.e., rovibrational and pre-dissociative states of the initial anion are actively present as the bound electron is moved into the continuum by the laser beam. The analysis of the PD mechanism for molecular negative ions also provides an important tool for the studies of reaction dynamics, where one wants to employ the initial anionic partner in
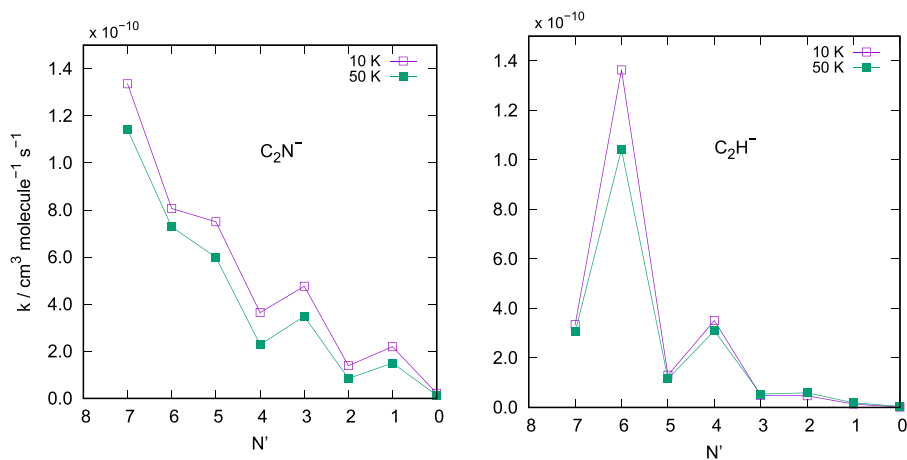
FIG. 8. Size changes of rotationally inelastic collisional rates for the C_2N^- (left panel) and the C_2H^- (right panel) anions. The two curves in each panel refer to two different temperatures as reported in the captions. The rates are calculated from the $N = 8$ state in each molecule, at the two temperatures shown, and the downward rates are given as a function of the final state for each anion (see the main text for further discussion).

a reaction to be specifically produced in a given rovibrational state of its ground electronic state as the neutral is generated in the PD reaction.

This process follows this sequence of events: (i) collisional population re-distribution among the rotational levels of the anion loaded in the trap and interacting with He, as the prevalent buffer gas, at a given trap temperature, and (ii) switching on of the photo-detaching laser after the previous rotational population equilibration has been achieved. One could then decide to vary the laser's operational wavelength to selectively depopulate different rotational states of the anion present in the trap after step (i), producing the ejected electron either at the threshold or away from it, or simply follow the total anion losses in the trap during the photo-detachment (PD) step; (iii) test the dynamical effects from changing other operating conditions such as buffer gas density, trap equilibration temperature, laser power, and laser wavelength in order to find the best choices for the PD processes tailored to the specific systems.

To follow the above steps in modeling the PD process, the state-changing collisional rates for the molecular anion of interest need to be known at different operating temperatures. Furthermore, we need to know as best as possible the PD rates (obtained from the PD cross sections as functions of the initial rotational state, as we have previously discussed[48,65]). As a comment about the calculated cross sections and rates for state-to-state inelastic processes, it suffices to say that the dominant inelastic processes we found for the present systems are those for which the state-changing values of $\Delta N \pm 1, 2$ and for which the rates at a temperature of, say 20 K, are of the order of 10^{-10} in units of cm^3 s^{-1}. As a comparison, the corresponding spontaneous emission Einstein A coefficients for the C_2H^- anion (in units of s^{-1}) vary to be from about 10^{-3} to 10^{-5} times smaller than the collisional rate constants for this system.[48] We shall therefore chiefly consider only collision-induced effects in the present analysis.

For modeling the rotational population evolution dynamics, the master equations need to be solved using the collisional thermal rates already computed above, at each chosen trap temperature and for the range of selected He density, which are expected to be experimentally achieved,

$$\frac{dn_i(t)}{dt} = \sum_{j \neq i} n_j(t) C_{ji}(T) - n_i(t) \left(\sum_{i \neq j} P_{ij}(T) + K_i^{PD} \right). \quad (3)$$

The quantities $P_{ij}(T)$ are the rates for the destruction of level i, while its formation rates are given by the $C_{ji}(T)$ terms. During the collisional step, i.e., before the laser is switched on, the coefficients are given as $P_{ij}(T) = \eta_{He} k_{i \rightarrow j}(T)$ and $C_{ji}(T) = \eta_{He} k_{j \rightarrow i}(T)$. These relationships describe the "collision-driven" time evolution process of thermalization of the relative populations of the rotational levels of the anion, which are reached at the selected buffer gas temperature and for a given density η_{He} in the trap. Once thermalization is reached and the PD laser is turned on, K_i^{PD} is the additional destruction rate of the selected level i caused by the PD laser. The set of rates K_i^{PD} is critical in the experiments, in general, and for the present numerical simulations because they drive the destruction of both the population of one specific rotational level i and of all the molecular

ions, which have been populating that specific state during the previous thermalization step in the traps. As the trapped anion is still undergoing collisions with the buffer gas, there is now competition between the laser-induced de-population of a rotational level and its collisional re-population in the trap.

In the experiments of this study, these rates depend on the laser photon flux and on the overlap between the laser beam and the ion cloud within the trap. Since these parameters, as well as the absolute values of the state-to-state PD cross sections, are presently unknown for the title molecular anions, we shall introduce a scaling parameter that we have already discussed in our earlier work[48,65–67] according to which the relation between the required rate and the estimated cross section is given by

$$K_N^{PD} = \alpha(\nu) \sigma_N^{PD}(\nu). \quad (4)$$

The above scaling parameter $\alpha(\nu)$ accounts globally for modeling the relative role of different features of the photo-detachment experiment, which are effectively the laser-driven features of the PD dynamics. They include quantities such as laser-flux and spatial overlap, which compete with the pure collisional rates that repopulate the anion's rotational levels via its interaction with the buffer gas. The specific scaling of that parameter within the modeling allows us to simulate either a "collision-dominated" situation or a "PD-dominated" situation whenever the laser strength is markedly varied by taking the $\alpha(\nu)$ to be either equal to 1.0 or one or more orders of magnitude smaller, as shown in our earlier work[48,65–67] and as discussed below. The values of $\sigma_N^{PD}(\nu)$ can be obtained through an analysis that we have presented before.[48,65–67] Briefly, the PD cross section is given as

$$\sigma_N^{PD}(\nu) \propto \sum_{N'=0}^{N_{max}} \left| C_{N010}^{N'0} \right|^2 (E - E_{th})^p \Theta(E - E_{th}). \quad (5)$$

Here, $\Theta(E - E_{th})$ is a step function so that only transitions with $E_{th} < E$ are considered, and the Clebsch–Gordan coefficient enforces the selection rule $\Delta J'' = \pm 1$ for the specific PD process under consideration. Since the rotational levels' relative populations initially also sum to one, they have a limited effect on the relative sizes of the PD cross sections and the PD curve identified by the above equation. Hence, the most important factors are the selected value for the p exponential parameter, a factor linked to the dipole selection rules of the photon-induced electron detachment and to the dominant partial wave (angular momentum) of the ejected electron, as discussed in Refs. 48 and 65–67. The actual wavelength ν of the laser source with respect to the threshold of the specific electron-detachment process is also an important feature in the discussion of the PD processes, as we shall further show below.

Following the prescription indicated in Eq. (5), we have calculated the relative values of the photo-detachment cross sections for the C_2N^- anion. The data for the C_2H^- anion we use here for comparison were presented before,[48,66] and therefore, we shall only discuss them during the analysis of the compared data below.

Tables I and II report three different choices for the exponential parameter already defined in the equation for the photo-detachment

cross section. They were chosen according to what is known about the experimental findings on the C_2N^- anion, as discussed, for example, in Ref. 43. Briefly, the photo-detachment process originates from the linear anion in its $(X^3\Sigma^-)$ electronic ground state with a molecular orbital (MO) configuration given as (core) $\pi^4 \sigma^2 \pi^2$. Removal of an electron from the highest occupied π or σ MO produces the neutral $(X^2\Pi)$ or neutral $(a^4\Sigma^-)$ final states since they are both accessible from the initial anionic states. As already shown in previous work,[43,46] photo-detachment from a π or σ MO at threshold energies can be mainly described as proceeding via either $s + d$ partial-wave contributions from the ejected electron or via a p-wave scattering contribution. Accordingly to the previous definition of the PD cross section, we can then assign to each of the outgoing electron channels different values of the exponential parameter $p = 0.5$ for s-wave scattering, 1.5 for p-wave scattering, and 2.5 for d-wave scattering. These two tables therefore report our relative estimates of the cross sections for all three possible values of the exponential parameter. The data in Table I present our results for the case in which the laser frequency is chosen to be resonant with the value of the electron affinity (EA) for the present anion, while the data in Table II indicate the cross section values when the laser frequency is increased by 50 cm^{-1} above threshold. The data clearly indicate that the relative values of the PD cross sections are affected by both the initial value of the anion rotational state N and the specific dominant partial wave for the outgoing electron. Such a difference will be clearly reflected in the dynamical modeling of the loss rates in the trap that we will further present below.

The computational results for the case of the C_2H^- anion in the trap were already reported earlier by us in previous work[48,66] and will not be repeated here. New calculations have been carried out for comparison and are given for the C_2N^- anion by the four panels shown in Fig. 9. The laser action is switched on after 5 s, which is well beyond the time needed for the collisional equilibration of the populations of the rotational levels to the temperature of the trap of 15 K. Earlier experiments[43] indicate that two peaks are associated with the transitions to the neutral $(X^2\Pi)$ state due to the splitting into two spin–orbit components. In the case of the C_2N, this splitting was found to be 38 cm^{-1}, close to earlier estimates and calculations of 40 cm^{-1}. We shall not include this value in estimating the energy of the ejected electron since the EA value

TABLE II. Same data as in Table I. Relative values of $\sigma_N^{PD}(\nu)$ as a function of p for ν = EA + 50 cm^{-1}.

N	$p = 0.5$	$p = 1.5$	$p = 2.5$
0	1.000	1.000	0.934
1	0.999	0.999	0.935
2	0.999	0.999	0.936
3	0.999	0.999	0.938
4	0.999	0.999	0.940
5	0.998	0.999	0.942
6	0.997	0.999	0.946
7	0.996	0.999	0.947

is much larger (i.e., around 2.75 eV) and the location of the upper $(a^4\Sigma^-)$ is about 9000 cm^{-1} above the lower $(X^2\Pi)$ neutral state. The photo-detachment process into the latter neutral product will therefore involve at the threshold the p values of either 0.5 or 2.5. The data presented in Fig. 9 in three of the panels show changes in trap operation for the case of s-wave scattering, while all three options for the p parameter are reported in the lower-right panel of the same figure to compare their effects on the total anion loss rates.

The most dramatic difference with the earlier studies we have done on the PD population evolutions in small molecular anions in cold traps[48,65–67] is the far higher number of populated rotational states of C_2N^- even at the low temperature of 15 K in the trap. In the data shown in all panels, the laser frequency has been kept resonant with the molecular EA of 2.7489 eV and the density of the buffer gas kept constant at 10^{10} cm^{-3}. The upper left panel employs the p exponent at 0.5, a value corresponding to the expected threshold behavior of the ejected electron from the ground $(X^3\Sigma^-)$ state of the anion undergoing photo-detachment of its outer π MO into a free electron at threshold energy and the $(X^2\Pi)$ state of the neutral. We see that all rotational states up to $N = 8$ are populated after collisional equilibration of the molecular rotational state population within the trap. On the reported time scale, the PD laser is switched on at $t = 0$ and the first 5 s evolution of fractional population losses is shown. We clearly see that essentially a uniform exponential decay if followed separately by each of the populated states in the trap.

As a different p exponent value is chosen, however, we see that the photo-detachment loss rates on the upper right panel correspond now to a threshold electron being ejected from an outer σ orbital of the initial anion into a free electron plus the next $(a^4\Sigma^-)$ state of the final neutral molecule. Here, the loss rates evolve much more slowly, and on the same time scale, we see that their relative populations remain much higher in the trap. Such differences of behavior should be amenable to detection in possible experiments. When the p exponent is further changed to the value corresponding to the higher energy component in the partial-wave expansion of the ejected electron from an outer π MO into the $(X^2\Pi)$ ground electronic state of the neutral molecule, we see from the changes of fractional populations of the rotational states populated initially at 15 K (lower-left panel of this figure) that the decay rates become even smaller and some of the higher rotational states are hardly depleted

TABLE I. Relative values of $\sigma_N^{PD}(\nu)$ for C_2N^- as a function of the rotational state N, given by the first column, and the different p values reported by the next three columns. The value of ν is fixed to be that of the electron affinity (EA) at 2.7489 eV.

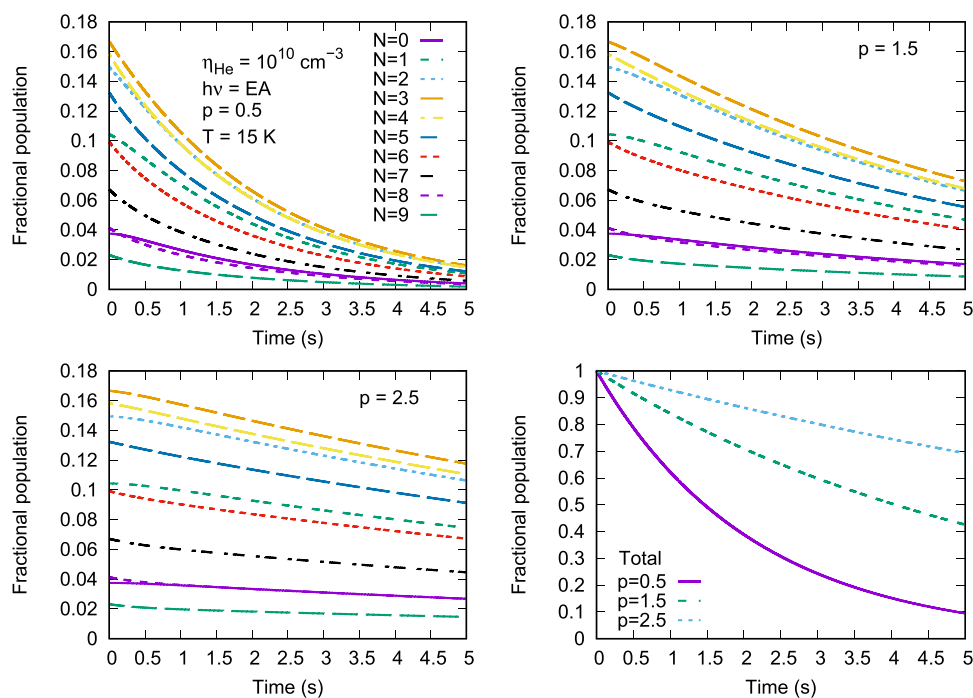| N	$p = 0.5$	$p = 1.5$	$p = 2.5$
0	0.00	0.00	0.00
1	0.23	0.03	0.003
2	0.35	0.06	0.01
3	0.44	0.11	0.03
4	0.51	0.16	0.05
5	0.58	0.22	0.08
6	0.64	0.28	0.12
7	0.69	0.35	0.18

FIG. 9. Computed population evolution results for the PD process for the case of the C_2N^- anion. Different operating conditions are shown in the panels, while the lower right panel reports all the changes in the total loss rates as the exponent p is modified in estimating the PD cross sections used to generate the rates (see the main text for further details).

during the shown time interval that was essentially emptying them in the data of the upper-left panel. This clearly indicates that the dominant partial-wave component for the ejected electron markedly affects the photo-detachment efficiency described by the value of the PD rates included in the previous set of coupled evolutionary equations.

A summary of such effects is presented in the lower-right panel of Fig. 9, where the total values of the fractional population losses are given for the three different choices of the p exponent in the expression for the PD cross section shown earlier. We clearly see the marked differences in the rate losses within the allotted time interval, indicating again that such differences in trap depletion behavior could be experimentally detectable.

Another interesting comparison is reported in the four panel of Fig. 10 where we compare the laser-induced population losses in the traps for two different values of the buffer gas density: on the two left panels, this value is kept at 10^{10} cm^{-3}, while the data in the two left panels are taken to be 10^{11} cm^{-3}. The laser frequencies are selected to be resonant with each of the chosen molecules in the data reported by the two panels on the left of this figure, while the data in the two panels on the right show an increase in the laser photo-detachment energy by 50 cm^{-1}. Besides showing the variations of the computed global losses when varying the operational conditions of the trap for the two title anions, we have also added as a comparison the results we have obtained for another system studied in photo-detachment experiments in traps: the CN^- anion that we have discussed in some of our recently submitted work.[36,67] The latter anion is a closed-shell, ($^1\Sigma$) molecule with a permanent dipole moment of 0.709 D. Its EA value has been recently measured very

accurately to be 3.6843(2) eV,[67] and at the threshold, the process is considered to chiefly give rise to an s-wave scattering electron modified by the dipole of the anion so that a value of the p exponent of around 0.44 can be realistically chosen, as discussed in an upcoming publication.[67]

The upper-left panel of Fig. 10 presents two choices for the present C_2N^- anion of the p exponent describing its PD cross section energy dependence and associated with the dominant s-wave and dominant p-wave behavior of the ejected electron at the threshold, as already discussed earlier. For the C_2H^- anion, the threshold behavior of the ejected electron is known to be chiefly controlled by p-wave scattering,[46] and therefore, the total loss rates reported in this panel employ the $p = 1.5$ exponential value. It is also interesting to note that the permanent dipole moments, involved in the evaluation of the transition moments defining the PD cross sections, show the largest value (3.09 D) for the C_2H^- anion, followed by the C_2N^- (2.18 D), and then by the CN^- (0.709 D). However, these values are not dominating the PD process in the trap since collisional efficiency and density of rotational states in the three systems are also important contributors. Thus, we see that the slowest anion losses in time occur for the two largest exponents describing the dominant partial waves of the ejected electrons. On the other hand, the two cases where at threshold s-wave scattering dominates exhibit here faster anion losses in the trap.

This relative behavior is also maintained by the data seen in the upper-right panel of Fig. 10: the trap setting, which has been changed, is the density of the buffer gas atoms, thus making the PD process to be driven by the increased collision
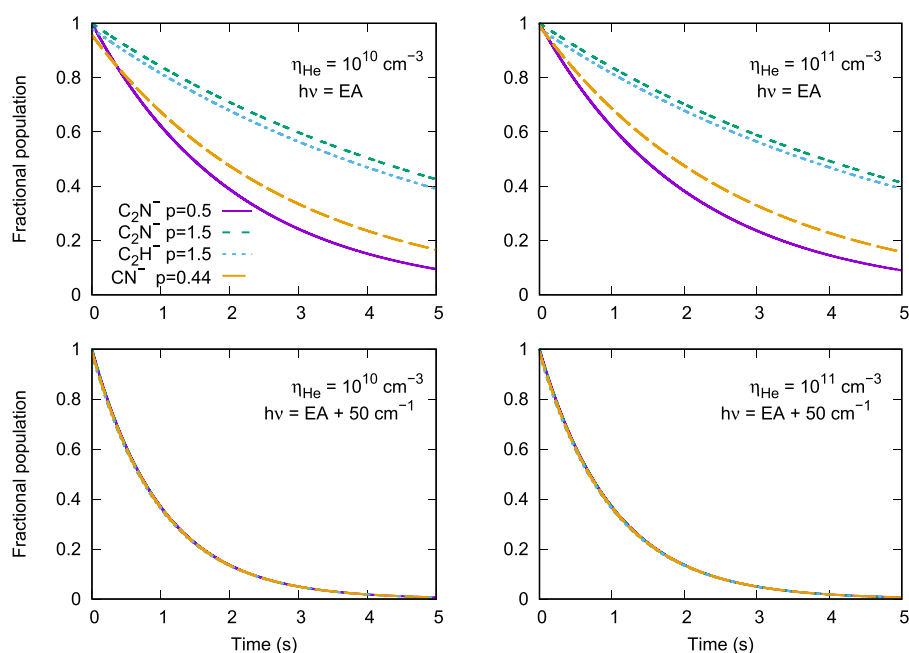
FIG. 10. A comparison of the computed results for the PD-induced rotational population decays for three different polar anions reported in the captions, under different trap conditions. The trap temperature is set to 15 K, while the two top panels select the laser frequency to be resonant with each EA value of the anion. In the lower two panels, the laser frequency is more energetic by 50 cm^{-1} (see the main text for further details).

numbers and the increased role of the collisional repopulations of the rotational states of the trapped molecule, referred to earlier as a "collision-dominated" photo-detachment process. We can therefore say that the more important differences between similar molecular anions are linked to their structural properties that decide the dominant partial wave during the threshold ejection of the extra electron.

As the photon energy is increased well above the EA thresholds in each system, as shown in the lower two panels of Fig. 10, we see how remarkably the anion losses are driven by the energetics of the laser and not by the structural features of the individual target: the present examples now exhibit markedly higher rates of decaying fractional populations of their anions. Additionally, the rates are the same for all of them without having their structural differences playing any significant role during the trap processes. We also clearly see that increasing the presence of collisional effects (in the lower-right panel) does not have any significant role in modifying the anion loss rates. In all the present systems, we also note that a single exponential decay can describe their rates, indicating that no structural features involving relative re-population between different rotational states are important enough to modify the rates during decay processes. This fact was also indicated by the individual decay rates shown by different rotational states of the C$_2$N$^-$ anion shown in the panels of Fig. 9. At the considered trap conditions of temperature, much fewer rotational states (i.e., up to $j = 3$) are significantly populated for the C$_2$H$^-$ anion and for the CN$^-$ anion (also up to $j = 3$).

Finally, by changing the value of α in Eq. (4), the time for anion loss for PD is modified. This accounts for details of a PD experiment as shown in our previous study of PD processes involving the *ortho*-NH$_2^-$ and *para*-NH$_2^-$ anions[65] where the

value of α was scaled to experimental ion losses. An order of magnitude decrease in the value of α leads to an order of magnitude increase in trap time. Thus, our calculations also find that for α values scaled down to 0.1 or 0.01, the survival of anions in the traps can be extended up to hundreds of seconds for the present systems.

V. CONCLUSIONS

In this work, we have analyzed in detail the structural features of the interaction potential energy between He atoms and two small linear anions, which have been often considered to be present (albeit not yet detected) in ISM when modeling the chemistry of such an environment, C$_2$H$^-$ ($X^1\Sigma^-$) and C$_2$N$^-$ ($X^3\Sigma^-$). We have employed the *ab initio* computed PESs to further evaluate the network of state-changing cross sections involving their lower rotational states in each of these systems, which would be significantly populated at the expected temperatures of interstellar conditions. The computed cross sections were then employed to obtain the corresponding state-changing rates over a range of temperatures also significant for interstellar environments. The calculations found different relative sizes between rates in both systems and the preference of transitions involving the $\Delta N = 2$ selection rule for the C$_2$H$^-$ anion, while transitions with $\Delta N = 1$ are dominating for the C$_2$N$^-$ anion. These differences of behavior can be linked to the structural differences between coupling dynamical terms in the interaction potentials, which guide rotational state-changing collisions for either molecular anion. Differences in propensity rules involving transitions with larger ΔN values also indicate that the C$_2$N$^-$ anion would favor transitions with odd values of ΔN, while the even values are those favored for C$_2$H$^-$. On the whole, however, our

calculations find that both anions behave similarly in terms of efficiency of collisional state-changing probabilities, while specific differences between processes are clearly present and can be amenable to observations.

We have also modeled the behavior of both molecular anions when uploaded to cold temperature ion traps (e.g., for temperatures around 15 K as an example) and using He as a buffer gas in the traps. In particular, we have modeled the photo-detachment processes of both anions after collisional equilibrium of their populated rotational states at the trap temperature. By modifying trap operating conditions such as the density of the buffer gas, the energy of the photo-detaching laser, and its power via scaling the corresponding PD rates driven by the laser, we have found differences of behavior between the two systems and indicated their crucial role in controlling the global loss rates of trapped anions of the dominant partial wave of the ejected threshold electron. The latter parameter depends on the selection rules of the PD process and on the initial and final electronic states of the anionic and of the final neutral molecule. The increase in the photon energy of the laser is also significantly affecting the loss rates and is seen in our modeling that can shift operating conditions from being either chiefly collision-driven events or laser-driven events, as we have already discussed in our earlier work.[48,66]

The availability of accurately determined state-changing rotational rates at the temperature of the ISM for molecular ions employed in these networks is expected to document more realistically the values for such quantities within kinetic models of chemical processes and energy exchange processes in this environment. We also suggest that our specific results for estimating the rates of ion loss changes in cold ion traps under different trap conditions could help in the preparation of future experiments on these anions.

SUPPLEMENTARY MATERIAL

See the supplementary material for the V_λ multipolar coefficients for the C_2N^-/He PES, the computed rates for C_2H^-/He, the computed rates for C_2N^-/He, and a *readme* file explaining the format and units of the rates. The supplementary material also contains a Fortran routine for the C_2N^-/He potential energy values of the new PES.

ACKNOWLEDGMENTS

DATA AVAILABILITY

The data that supports the findings of this study are available within the article (and its supplementary material).

REFERENCES

[1]M. A. Cordiner, T. J. Millar, C. Walsh, E. Herbst, D. C. Lis, T. A. Bell, and E. Roueff, "Organic molecular anions in interstellar and circumstellar environments," Proc. Int. Astron. Union **4**, 157–160 (2008).

[2]M. A. Cordiner and T. J. Millar, "Density-enhanced gas and dust shells in a new chemical model for IRC+10216," Astrophys. J. **697**, 68 (2009).

[3]T. J. Millar, C. Walsh, and T. A. Field, "Negative ions in space," Chem. Rev. **117**, 1765–1795 (2017).

[4]E. Herbst and Y. Osamura, "Calculations on the formation rates and mechanisms for C_nH anions in interstellar and circumstellar media," Astrophys. J. **679**, 1670 (2008).

[5]C. Walsh, N. Harada, E. Herbst, and T. J. Millar, "The effects of molecular anions on the chemistry of dark clouds," Astrophys. J. **700**, 752 (2009).

[6]B. Eichelberger, T. P. Snow, C. Barckholtz, and V. M. Bierbaum, "Reactions of H, N, and O atoms with carbon chain anions of interstellar interest: An experimental study," Astrophys. J. **667**, 1283 (2007).

[7]T. Best, R. Otto, S. Trippel, P. Hlavenka, A. von Zastrow, S. Eisenbach, S. Jézouin, R. Wester, E. Vigren, M. Hamberg, and W. D. Geppert, "Absolute photodetachment cross-section measurements for hydrocarbon chain anions," Astrophys. J. **742**, 63 (2011).

[8]N. Douguet, V. Kokoouline, and A. E. Orel, "Photodetachment cross sections of the $C_{2n}H^-$ ($n = 1$–3) hydrocarbon-chain anions," Phys. Rev. A **90**, 063410 (2014).

[9]A. Dalgarno and R. A. McCray, "The formation of interstellar molecules from negative ions," Astrophys. J. **181**, 95 (1973).

[10]E. Herbst, "Can negative molecular ions be detected in dense interstellar clouds?," Nature **289**, 656 (1981).

[11]M. C. McCarthy, C. A. Gottlieb, H. Gupta, and P. Thaddeus, "Laboratory and astronomical identification of the negative molecular ion C_6H^-," Astrophys. J. **652**, L141 (2006).

[12]K. Kewaguchi, Y. Kasai, S.-I. Ishikawa, and N. Kaifu, "A spectral-line survey observation of IRC +10216 between 28 and 50 GHz," Publ. Astron. Soc. Jpn. **47**, 853 (1995).

[13]J. Cernicharo, M. Guélin, M. Agúndez, K. Kawaguchi, M. McCarthy, and P. Thaddeus, "Astronomical detection of C_4H^-, the second interstellar anion," Astron. Astrophys. **467**, L37 (2007).

[14]A. J. Remijan, J. M. Hollis, F. J. Lovas, M. A. Cordiner, T. J. Millar, A. J. Markwick-Kemper, and P. R. Jewell, "Detection of C_8H^- and comparison with C_8H toward IRC +10216," Astrophys. J. **664**, L47 (2007).

[15]S. Brünken, H. Gupta, C. A. Gottlieb, M. C. McCarthy, and P. Thaddeus, "Detection of the carbon chain negative ion C_8H^- in TMC-1," Astrophys. J. **664**, L43 (2007).

[16]P. Thaddeus, C. A. Gottlieb, H. Gupta, S. Brünken, M. C. McCarthy, M. Agúndez, M. Guélin, and J. Cernicharo, "Laboratory and astronomical detection of the negative molecular ion C_3N^-," Astrophys. J. **677**, 1132 (2008).

[17]J. Cernicharo, M. Guélin, M. Agúndez, M. C. McCarthy, and P. Thaddeus, "Detection of C_5N^- and vibrationally excited C_6H in IRC +10216," Astrophys. J. **688**, L83 (2008).

[18]M. Agúndez, J. Cernicharo, M. Guélin, C. Kahane, E. Roueff, J. Kłos, F. J. Aoiz, F. Lique, N. Marcelino, J. R. Goicoechea, M. González García, C. A. Gottlieb, M. C. McCarthy, and P. Thaddeus, "Astronomical identification of CN-, the smallest observed molecular anion," Astron. Astrophys. **517**, L2 (2010).

[19]N. Sakai, T. Shiino, T. Hirota, T. Sakai, and S. Yamamoto, "Long carbon-chain molecules and their anions in the starless core, Lupus-1A," Astrophys. J. **718**, L49 (2010).

[20]S. Brünken, C. A. Gottlieb, H. Gupta, M. C. McCarthy, and P. Thaddeus, "Laboratory detection of the negative molecular ion CCH^-," Astron. Astrophys. **464**, L33 (2007).

[21]T. Amano, "Extended negative glow and "hollow anode" discharges for submillimeter-wave observation of CN^-, C_2H^-, and C_4H^-," J. Chem. Phys. **129**, 244305 (2008).

[22]K. D. Tucker, M. L. Kutner, and P. Thaddeus, "The ethynyl radical C_2H—A new interstellar molecule," Astrophys. J. **193**, L115 (1974).

[23]C. Barckholtz, T. P. Snow, and V. M. Bierbaum, "Reactions of C_n^- and C_nH^- with atomic and molecular hydrogen," Astrophys. J. **547**, L171 (2001).

[24] A. Spielfiedel, N. Feautrier, F. Najar, D. Ben Abdallah, F. Dayou, M. L. Senent, and F. Lique, "Fine and hyperfine excitation of C_2H by collisions with He at low temperature," Mon. Not. R. Astron. Soc. **421**, 1891 (2012).

[25] P. J. Dagdigian, "Hyperfine excitation of C_2H in collisions with *ortho*- and *para*-H_2," Mon. Not. R. Astron. Soc. **479**, 3227 (2018).

[26] F. Dumouchel, F. Lique, A. Spielfiedel, and N. Feautrier, "Hyperfine excitation of C_2H and C_2D by *para*-H_2," Mon. Not. R. Astron. Soc. **471**, 1849 (2017).

[27] F. Dumouchel, A. Spielfiedel, M. L. Senent, and N. Feautrier, "Temperature dependence of rotational excitation rate coefficients of C_2H^- in collision with He," Chem. Phys. Lett. **533**, 6 (2012).

[28] M. L. Senent, F. Dayou, F. Dumouchel, C. Balança, and N. Feautrier, "Inelastic rate coefficients for collisions of C_4H^- with *para*-$H_2(j = 0)$ at low temperatures," Mon. Not. R. Astron. Soc. **486**, 422 (2019).

[29] K. M. Walker, F. Lique, and R. Dawes, "Fine and hyperfine collisional excitation of C_6H by He," Mon. Not. R. Astron. Soc. **473**, 1407 (2017).

[30] K. M. Walker, F. Lique, F. Dumouchel, and R. Dawes, "Inelastic rate coefficients for collisions of C_6H^- with H_2 and He," Mon. Not. R. Astron. Soc. **466**, 831 (2016).

[31] F. Lique, A. Spielfiedel, N. Feautrier, I. F. Schneider, J. Kłos, and M. H. Alexander, "Rotational excitation of $CN(x^2\sigma^+)$ by He: Theory and comparison with experiments," J. Chem. Phys. **132**, 024303 (2010).

[32] F. Lique and J. Kłos, "Hyperfine excitation of CN by He," Mon. Not. R. Astron. Soc. **413**, L20–L23 (2011), http://oup.prod.sis.lan/mnrasl/article-pdf/413/1/L20/4895585/413-1-L20.pdf.

[33] Y. Kalgina, F. Lique, and J. Kłos, "Hyperfine collisional rate coefficients of CN with $H_2(j = 0)$," Mon. Not. R. Astron. Soc. **422**, 812 (2012).

[34] Y. Kalgina, J. Kłos, and F. Lique, "Collisional excitation of $CN(X^2\Sigma^+)$ by *para*- and *ortho*-H_2: Fine-structure resolved transitions," J. Chem. Phys. **139**, 074301 (2013).

[35] J. Kłos and F. Lique, "First rate coefficients for an interstellar anion: Application to the CN^--H2 collisional system," Mon. Not. R. Astron. Soc. **418**, 271–275 (2011).

[36] L. González-Sánchez, B. P. Mant, R. Wester, and F. A. Gianturco, "Rotationally inelastic collisions of CN^- with He: Computing cross sections and rates in the interstellar medium," Astrophys. J. (in press) (2020).

[37] M. Lara-Moreno, T. Stoecklin, and P. Halvick, "Rotational (de-) excitations of C_3N^- by collisions with He atoms," Mon. Not. R. Astron. Soc. **467**, 4174 (2017).

[38] M. Lara-Moreno, T. Stoecklin, and P. Halvick, "Rotational transitions of C_3N^- induced by collision with H_2," Mon. Not. R. Astron. Soc. **486**, 414 (2019).

[39] T. Tchakoua, O. Motapon, and M. Nsangou, "Cross-sections and rate coefficients calculations for rotational excitation of cyanoethynylide ions (C_3N^-) induced by collision with He atoms at low temperature," J. Phys. B: At. Mol. Opt. Phys. **51**, 045202 (2018).

[40] B. Bastian, T. Michaelsen, J. Meyer, and R. Wester, "Anionic carbon chain growth in reactions of C_2^-, C_4^-, C_6^-, C_2H^-, C_4H^-, and C_6H^- with C_2H_2," Astrophys. J. **878**, 162 (2019).

[41] J. K. Anderson and L. M. Ziurys, "Detection of CCN ($x^2\pi_r$) in IRC+10216: Constraining carbon-chain chemistry," Astrophys. J. **795**, L1 (2014).

[42] K. Kawaguchi, T. Suzuki, S. Saito, E. Hirota, and T. Kasuya, "Dye laser excitation spectroscopy of the CCN radical," J. Mol. Spectrosc. **106**, 320 (1984).

[43] E. Garand, T. I. Yacovitch, and D. M. Neumark, "Slow photoelectron velocity-map imaging spectroscopy of C_2N^-, C_4N^-, and C_6N^-," J. Chem. Phys. **130**, 064304 (2009).

[44] X. Huang and T. J. Lee, "Accurate *ab initio* quartic force fields for NH_2^- and CCH^- and rovibrational spectroscopic constants for their isotopologs," J. Chem. Phys. **131**, 104301 (2009).

[45] K. M. Ervin and W. C. Lineberger, "Photoelectron Spectra of C_2^- and C_2H^-," J. Phys. Chem. **95**, 1167 (1991).

[46] J. Zhou, E. Garand, and D. M. Neumark, "Vibronic structure of C_2H and C_2D from anion slow electron velocity-map imaging spectroscopy," J. Chem. Phys. **127**, 114313 (2007).

[47] M. L. Senent and M. Hochlaf, "Reactivity of anions in interstellar media: Detectability and applications," Astrophys. J. **768**, 59 (2013).

[48] F. A. Gianturco, L. González-Sánchez, B. P. Mant, and R. Wester, "Modelling state-selective photodetachment in cold ion traps: Rotational state "crowding" in small anions," J. Chem. Phys. **151**, 144304 (2019).

[49] H.-J. Werner, P. J. Knowles, G. Knizia, F. R. Manby, and M. Schütz, "Molpro: A general-purpose quantum chemistry program package," Wiley Interdiscip. Rev.: Comput. Mol. Sci. **2**, 242–253 (2012).

[50] H.-J. Werner, P. J. Knowles, G. Knizia, F. R. Manby, M. Schütz *et al.*, Molpro, version 2019.2, a package of *ab initio* programs, 2019, see https://www.molpro.net.

[51] D. E. Woon and T. H. Dunning, "Gaussian basis sets for use in correlated molecular calculations. IV. Calculation of static electrical response properties," J. Chem. Phys. **100**, 2975 (1994).

[52] H.-J. Werner and P. J. Knowles, "An efficient internally contracted multiconfiguration-reference configuration interaction method," J. Chem. Phys. **89**, 5803 (1988).

[53] K. R. Shamasundar, G. Knizia, and H.-J. Werner, "A new internally contracted multi-reference configuration interaction method," J. Chem. Phys. **135**, 053101 (2011).

[54] S. R. Langhoff and E. R. Davidson, "Configuration interaction calculations on the nitrogen molecule," Int. J. Quantum Chem. **8**, 61–72 (1974).

[55] J. Buenker and S. Peyeremhoff, "Ab initio calculations close to the full CI level of accuracyand their use for the interpretation of molecular spectra," in *New Horizons of Quantum Chemistry*, edited by P.-O. Lowdin and B. Pullman (D. Reidel Pub. Co., Dordrecht., 1982), pp. 183–219.

[56] M. Puchalski, K. Szalewicz, M. Lesiuk, and B. Jeziorski, "QED calculation of the dipole polarizability of helium atom," Phys. Rev. A **101**, 022505 (2020).

[57] D. López-Durán, E. Bodo, and F. A. Gianturco, "ASPIN: An all spin scattering code for atom-molecule rovibrationally inelastic cross sections," Comput. Phys. Commun. **179**, 821 (2008).

[58] R. Martinazzo, E. Bodo, and F. A. Gianturco, "A modified variable-phase algorithm for multichannel scattering with long-range potentials," Comput. Phys. Commun. **151**, 187 (2003).

[59] M. Hernández Vera, F. A. Gianturco, R. Wester, H. da Silva, Jr., O. Dulieu, and S. Schiller, "Rotationally inelastic collisions of H_2^+ ions with He buffer gas: Computing cross sections and rates," J. Chem. Phys. **146**, 124310 (2017).

[60] L. González-Sánchez, E. Bodo, and F. A. Gianturco, "Quantum scattering of OH ($x^2\pi$) with He (^1s): Propensity features in rotational relaxation at ultralow energies," Phys. Rev. A **73**, 022703 (2006).

[61] L. González-Sánchez, E. Bodo, and F. A. Gianturco, "Quenching of molecular ions by He buffer loading at ultralow energies: Rotational cooling of $OH^+(^3\sigma^-)$ from quantum calculations," Eur. Phys. J. D **44**, 65 (2007).

[62] L. González-Sánchez, R. Wester, and F. A. Gianturco, "Modeling quantum kinetics in ion traps: State-changing collisions for OH^+," ChemPhysChem **19**, 1866 (2018).

[63] M. H. Alexander and P. J. Dagdigian, "Propensity rules in rotationally inelastic collisions of diatomic molecules in $^3\sigma$ electronic states," J. Phys. Chem. **79**, 302 (1983).

[64] D. E. Manolopoulos, "An improved log derivative method for inelastic scattering," J. Chem. Phys. **85**, 6425 (1986).

[65] F. A. Gianturco, O. Y. Lakhmanskaya, M. H. Vera, E. Yurtsever, and R. Wester, "Collisional relaxation kinetics for *ortho* and *para* NH_2^- under photodetachment in cold ion traps," Faraday Discuss. **212**, 117–135 (2018).

[66] B. P. Mant, M. Nötzold, L. González-Sánchez, R. Wester, and F. A. Gianturco, " Rotational state selective C_2H^- losses from quantum dynamics," Eur. Phys. J. D (submitted) (2020).

[67] M. Simpson, M. Nötzold, T. Michaelsen, B. Bastian, J. Meyer, R. Wild, F. A. Gianturco, M. Milovanovic, V. Kokoouline, and R. Wester, "Threshold photo-detachment spectroscopy and modelling of the astrochemical anion CN^-" (unpublished) (2020).